INTERFACE FOCUS

rsfs.royalsocietypublishing.org

Research

Cite this article: Susilo ME, Paten JA, Sander EA, Nguyen TD, Ruberti JW. 2016 Collagen network strengthening following cyclic tensile loading. *Interface Focus* **6**: 20150088.
http://dx.doi.org/10.1098/rsfs.2015.0088

One contribution of 19 to a theme issue 'Integrated multiscale biomaterials experiment and modelling: towards function and pathology'.

Subject Areas:
bioengineering, biomaterials, biomechanics

Keywords:
collagen network, mechanical adaptation, tissue remodelling

Author for correspondence:
Jeffrey W. Ruberti
e-mail: j.ruberti@neu.edu

THE ROYAL SOCIETY PUBLISHING

Collagen network strengthening following cyclic tensile loading

Monica E. Susilo[1], Jeffrey A. Paten[1], Edward A. Sander[2], Thao D. Nguyen[3] and Jeffrey W. Ruberti[1]

[1]Bioengineering, Northeastern University, Boston, MA 02115, USA
[2]Biomedical Engineering, University of Iowa, Iowa City, IA 52242, USA
[3]Mechanical Engineering, Johns Hopkins, Baltimore, MD 21218, USA

The bulk mechanical properties of tissues are highly tuned to the physiological loads they experience and reflect the hierarchical structure and mechanical properties of their constituent parts. A thorough understanding of the processes involved in tissue adaptation is required to develop multiscale computational models of tissue remodelling. While extracellular matrix (ECM) remodelling is partly due to the changing cellular metabolic activity, there may also be mechanically directed changes in ECM nano/microscale organization which lead to mechanical tuning. The thermal and enzymatic stability of collagen, which is the principal load-bearing biopolymer in vertebrates, have been shown to be enhanced by force suggesting that collagen has an active role in ECM mechanical properties. Here, we ask how changes in the mechanical properties of a collagen-based material are reflected by alterations in the micro/nanoscale collagen network following cyclic loading. Surprisingly, we observed significantly higher tensile stiffness and ultimate tensile strength, roughly analogous to the effect of work hardening, in the absence of network realignment and alterations to the fibril area fraction. The data suggest that mechanical loading induces stabilizing changes internal to the fibrils themselves or in the fibril–fibril interactions. If such a cell-independent strengthening effect is operational *in vivo*, then it would be an important consideration in any multiscale computational approach to ECM growth and remodelling.

1. Introduction

The application of mechanical loading to soft connective tissues *in vivo* can alter the tissue's properties in the long term. Athletic training, for instance, can trigger tendon tissue adaptation [1–3], whereas repetitive overloading and overuse can induce progressive microstructural damage which causes mechanical fatigue [4,5]. An absence of physiological mechanical stimulation leads to atrophy and degradation of tissue mechanical properties [6]. Other than tissue maintenance, mechanical loading is also essential in development. For instance, the removal of intraocular pressure in chick eyes during embryonic development severely reduces eye growth [7]. In an *in vitro* study, the presence of anchors that allow mechanical contraction by tendon fibroblasts promotes the development of an embryonic-like collagenous matrix [8]. *In vivo*, the changes in tissue structure and mechanics over time can partly be attributed to cellular metabolic activity in response to dynamic mechanical stimulation, such as synthesis of extracellular matrix (ECM) protein molecules (e.g. collagen [9,10], proteoglycans [11]) and proteinases, such as the MMP family [12] which modify, replace or remove components of the ECM. However, even without the active involvement of cells, the intrinsic mechanical properties of the tissue itself can change with time and history of the applied loads [13].

Cyclic loading can cause dramatic changes in the stiffness and nonlinearity of the stress–strain behaviour of tendon, skin and other soft collagenous tissues [13–18]. The stress response is altered between the loading and unloading step, and also with each subsequent cycle [13]. Repeated cyclic loading causes the

stress–strain curves to shift to the right [14,15,19], and the peak force to decrease [14–16]. The extent that preconditioning changes the mechanical properties of soft tissues depends on the tissue system and the applied stress/deformation state [20]. This preconditioning effect stabilizes with each subsequent cycle to a repeatable reference state [13]. The application of cyclic loading may also alter the failure properties of tissue. Remarkably, an increase in the ultimate stress was observed after cyclic loading in tendons [17,18,21], ligaments [17,18] and collagen gels [22]. A study by Legerlotz *et al*. [23], however, showed a decrease in tendon ultimate stress as a result of cyclic loading. This inconsistency might have been caused by the application of cyclic loading with a high strain magnitude (more than half of the failure strain). The underlying mechanism that drives the tissue strengthening in response to cyclic loading is still not well understood. One possible source is the change in microstructure. Quinn *et al*. [16] showed small modifications in the fibre direction (approx. 11.4° rotation) after the application of cyclic loading, although this investigation did not report the ultimate stress. In another study by Tower *et al*. [24], cyclic loading of collagen tissue equivalent was shown to alter the collagen orientation only when the cyclic loading was force-controlled (the specimen was returned to preload in each cycle), whereas collagen orientation was recoverable when cyclic loading was displacement-controlled (the specimen was returned to zero displacement). The dependence of recoverable fibril orientation on whether the specimen was returned to preload or initial length was also observed in tendons in a study by Miller *et al*. [25], although both papers did not report the effect of preconditioning on the tissue failure properties. Both force-controlled and displacement-controlled cyclic loading showed a preconditioning-induced strengthening phenomenon [17,18,21,22], though, none of the studies measured collagen fibril orientation distribution post-cyclic loading. Therefore, it is unclear whether the tissue strengthening was as a result of fibril realignment. Cheema *et al*. [22] investigated collagen microstructure and found that tissue strengthening was accompanied by an increase in fibril diameter with increasing numbers of cycles.

Of the ECM proteins, collagen is the most abundant component in connective soft tissues, such as skin [26,27], cornea [28], sclera [29] and tendon [27]. It not only serves as the primary load-bearing structure in the tissue, but it also appears to be mechano-sensitive. The presence of mechanical load can stabilize collagen against enzymatic [30–36] and thermal [37,38] degradation. We hypothesize that the change of tissue mechanical properties from cyclic loading in the absence of cells is caused by direct structural alterations of collagen. Collagen originates in the cell as a nanoscale string that assembles into hierarchical structures which are orders of magnitude longer than the molecules from which they are derived. Thus, the structural organization at different hierarchical scales can affect the bulk mechanics of a network of collagen. We speculate that the structural alteration following mechanical loading includes not only the re-orientation of collagen fibrils in the collagen network towards the direction of load, but also a shift in collagen molecules towards the loaded fibrils.

We approach this investigation by employing a surrogate for natural ECM: a dense, disorganized collagen substrate (DDCS), which consists of a dense isotropic network of nearly pure type I collagen fibrils and permits the isolation of the response of collagen to the applied mechanical stimulation, without the influence of living cells, permanent cross-links and other extracellular components. The single component nature of this substrate is essential in this investigation, because this type of network will allow the direct comparison of the mechanical properties to the microstructural characteristics. Previous studies [39,40] have established that a non-woven fibrous network of non-interacting material, such as polyester felt or polypropylene fabric, possesses a stress–strain curve with similar characteristics to soft tissues: an initial low stiffness caused by the entropic rearrangement of the fibrils, followed by a higher stiffness at higher strain levels caused by the enthalpic deformation (bending and elongation) of the fibrillar material [41]. This type of network also generates a high Poisson's ratio [39] which has also been observed in connective tissue [42] and low concentration collagen gels under uniaxial loading [43]. The mechanical properties of such fibrous networks are regulated by the material properties of each fibril, the nature of the interfibrillar connections and the network architecture [40]. Because molecular mobility is not inhibited within the uncross-linked collagen network in DDCS, unlike the non-interacting nature of polyester or polypropylene, alteration in the mechanical properties of DDCS may be attributed to modification of any of these three factors.

Towards understanding the microstructural source of the adaptive mechanical properties of soft tissue, we first ask whether cyclic mechanical stimulation of a collagen network would induce network remodelling. The aim of this study was to characterize the changes in mechanical properties and network microstructure of the DDCS as a result of cyclic loading. The microstructure after cyclic loading was captured using transmission electron microscopy (TEM) in planes parallel and perpendicular to the loading direction, allowing direct visualization and analysis of the collagen network. Microstructural parameters such as collagen fibril orientation distribution, diameter distribution, area fraction and fibril D-periodicity were measured from the images.

2. Methods

2.1. Fabrication of the dense, disorganized collagen substrate

Pepsin-solubilized bovine collagen type I solution (PureCol, Advanced BioMatrix, Inc., Carlsbad, CA) was mixed with 10X phosphate-buffered saline (PBS) and 0.1 M sodium hydroxide in 8 : 1 : 1 ratio. The collagen concentration in this solution is 2.48 mg ml^{-1}. For optical deformation measurements, 7.5 µl of a 10 µm diameter polystyrene bead suspension (Polysciences, Inc. Warrington, PA) was mixed into the collagen solution. Using a syringe, 9 ml of the solution was transferred into a dialysis cassette (3500 MWCO slide-A-lyzer 3–12 ml model, Thermo Fisher Scientific, Inc., Rockford, IL). The cassette was incubated in a humid 37°C incubator for 3 h to allow for collagen self-assembly, and then immersed in 40% (w/v) 35,000 poly(ethylene) glycol (PEG) for 24 h to dehydrate and compress the collagen material into a thin sheet of randomly oriented fibrils in the *en face* plane (figure 1). After rinsing the cassette with 1X PBS to remove residual PEG solution, the centre portion of the DDCS sheet was cut into four approximately 5 × 15 mm strips using surgical scissors and sterilized by submerging in 70% ethanol for 30 min, followed by three washes of sterile 1X PBS. For consistency, DDCS specimens were tested within 6 h after

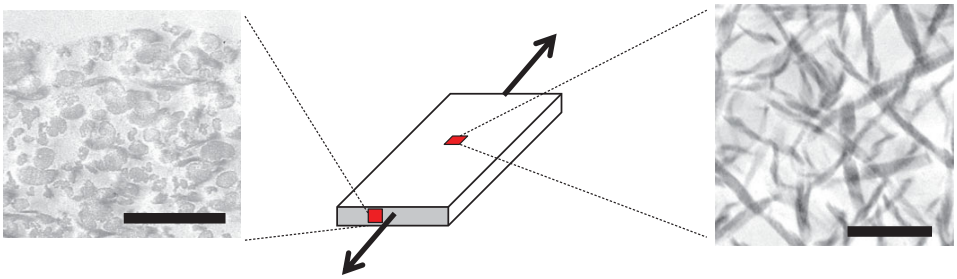

Figure 1. Dense, disorganized collagen substrate is a soft-tissue ersatz which was fabricated by dehydration against polyethylene glycol. The resulting product is a dense collagen sheet which is isotropic along the plane parallel to the surface. Scale bar, 1 μm. (Online version in colour.)

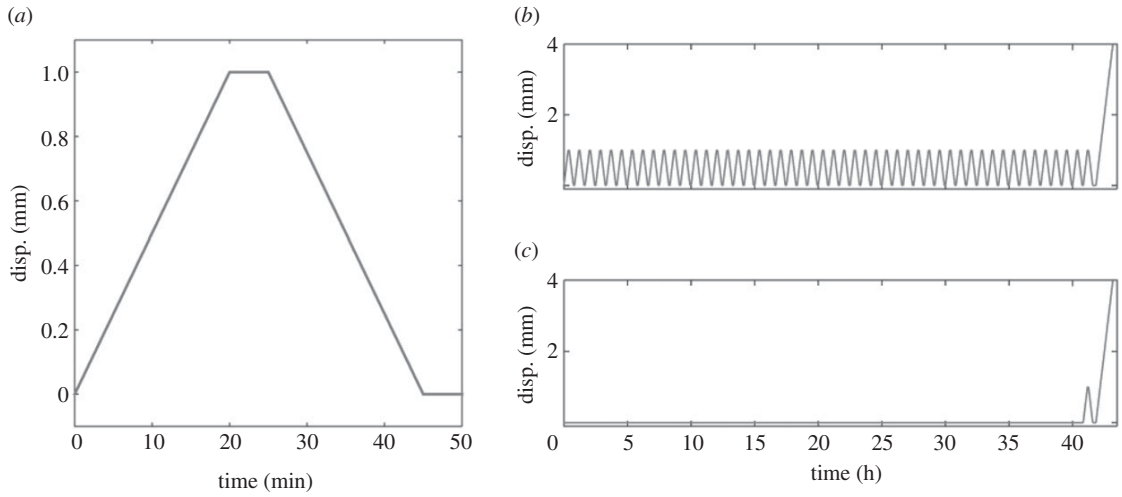

Figure 2. (*a*) In one-cycle period, the DDCS was loaded to a set maximum displacement magnitude (1 mm in this case), held at the maximum displacement, unloaded to zero displacement, and held at zero displacement. (*b*) After 50 cycles, the sample was loaded to failure. (*c*) In the one-cycle experimental groups, the cycle starts during the last cycle of the 50-cycle group before the sample was loaded to failure.

sterilization. Long-term storage of *in vitro* assembled collagen at room temperature and pressure has been shown to significantly increase the ultimate tensile strength [44]. The collagen concentration was estimated from the dimensions of the dialysis cassette and the dehydrated thickness (see method section on Transmission electron microscopy) to be 293 ± 89 mg ml^{-1}.

2.2. Mechanical testing and sample preparation

Mechanical testing was performed using a previously developed custom mechano-bioreactor [45]. The mechano-bioreactor allowed mechanical testing to be performed under controlled environmental conditions suitable for *in vitro* cell culture: at 37°C in 1X Dulbecco's modified Eagle's medium (GE Healthcare Life Sciences, Logan, UT) with 10% fetal bovine serum (Atlanta Biologicals, Flowery Branch, GA), 1% penicillin–streptomycin (GE Healthcare Life Sciences) and 0.1% amphotericin-B (Corning Inc., Corning, NY) conditioned with 5% CO_2. The medium was perfused using a syringe pump at a flow rate of 8 μl min^{-1}. Findings from previous studies have shown that testing temperature and solution medium can influence the measured mechanical behaviour. Meghezi *et al*. [46] measured a lower tangent modulus of collagen gel when the experiment was conducted at 37°C compared with room temperature. The force was measured using a 500 g load cell (Honeywell, Morristown, NJ) at a sampling rate of 1 Hz. The DDCS was mounted between two spring-loaded grips [45], and preloaded to 0.002 N. The reference length and width of the sample were measured, and the specimen was subjected to uniaxial tension cyclic loading. The length and width of the specimen was measured again following cyclic loading, and the specimens were subjected to a final loading to failure.

2.3. Cyclic strain protocol

The DDCS specimen was subjected to a displacement-controlled cyclic loading where each cycle consisted of a ramp loading for 20 min, a hold at maximum displacement for 5 min, a ramp unloading for 20 min and another hold at zero displacement for 5 min (figure 2). We examined two deformation levels: 1 and 2 mm, which corresponded to $13.0 \pm 1.1\%$ and $26.7 \pm 2.2\%$ strain. The lower strain level was well below the failure strain (at least three times smaller than the failure strain), and it corresponded to the linear region of the stress–strain curve. In the higher strain level group, the DDCS was likely to be stretched to a point where damage is likely occurring. At each deformation level, two groups were tested: one-cycle (control) and 50-cycle groups. Table 1 shows the experimental parameters for each group. The deformation rate for the two strain levels was different in order to obtain a consistent cycle period (50 min). The total length of cyclic loading was 41 h and 40 min. In the case of the one-cycle control groups, the DDCS was stored under the same environmental conditions as the 50-cycle group before starting the single cycle. We chose a low strain rate to achieve an equilibrium response. Following cyclic loading, the specimen was either subjected to a ramp load to failure protocol to determine the mechanical properties or fixed for TEM (table 1). The bioreactor was degassed to remove air bubbles, as needed, by flushing the chamber with a high flow rate. The force reading during the degassing cycle was excluded from the mechanical analysis.

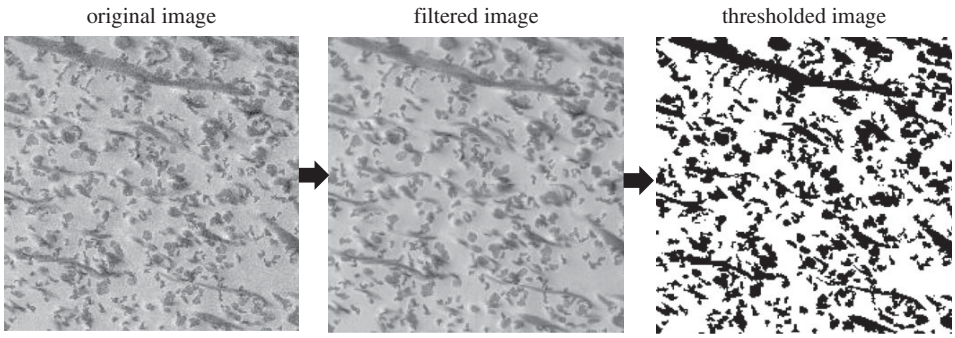

Figure 3. The sequence of image processing to obtain a binary image.

Table 1. Experimental parameters for each of the four groups tested.

displacement magnitude	1 mm		2 mm	
no. cycles	one	50	one	50
no. samples loaded to failure	6	6	6	6
no. samples for TEM	3	3	3	3
deformation rate during loading/unloading cycle (mm min^{-1})	0.05		0.10	
deformation rate during ramp to failure (mm min^{-1})	0.05		0.05	
cycle period (min)	50		50	

2.4. Mechanics data post-processing

During the cyclic loading experiment, a slow force drift up to 0.005 N can appear within 1 day. The force drift was removed by subtracting the force response of the current cycle by the force at zero displacement during the corresponding cycle, where the sample was visibly slack from the plastic deformation due to preconditioning. The engineering stress, σ, was defined as the measured force normalized by the initial cross-sectional area before cyclic loading and strain, ε, was defined as the grip displacement divided by the reference length before cyclic loading. The initial sample length was established by applying a 0.002 N preload, which corresponded to a 6 kPa pre-stress. Sample width at the centre point of the sample was measured using the calibrated microscope stage. Average initial sample thickness was measured from cross-sectional sections of three additional samples embedded in resin (see methods section on transmission electron microscopy). The stress-free displacement at each cycle was defined when the force reading equalled the preload of 0.002 N. The slope of the stress–stretch curve after cyclic loading was computed from the stress–strain data using finite difference. Data post-processing was performed in Matlab (MathWorks, Natick, MA).

2.5. Transmission electron microscopy

Three specimens for each experimental group were used for TEM characterization of the collagen fibril structure after cyclic loading. The collagen substrates were cut at the grips and immediately fixed in Karnovsky fixative at 4°C for at least 24 h and then washed with 0.1 M sodium cacodylate buffer (pH 7.2). The central 2 × 3 mm section of the specimen was cut to 0.5 × 1.5 mm strips. The strips were post-fixed with 1% osmium tetroxide in 0.1 M sodium cacodylate buffer for 2 h and washed again with 0.1 M sodium cacodylate buffer before undergoing the ethanol dehydration process. The strips were immersed in solutions with gradually increasing concentrations of ethanol from 35% to 95% for 15 min each and then immersed in 100% ethanol for 1 h with two changes of solution. The dehydrated strips were embedded in squetol resin and cut into 60–90 nm sections (silver–gold interference colour) using an ultramicrotome (LKB 8802A Ultrotome III, Sweden) in two directions, transverse and *en face* (figure 1). The sections were stained with 5% uranyl acetate and Reynold's lead citrate and imaged with a transmission electron microscope (JEOL JEM 1010 Electron Microscope, Peabody, MA).

The loading direction was tracked carefully when preparing the *en face* sections. The long axis of the strip always corresponded to the loading direction. Artefacts such as local compression and knife marks can develop during sectioning, and we used these artefacts to identify the loading direction. Polystyrene beads scattered within the DDCS were elliptical in shape due to the local compression during sectioning. The minor axis of the compressed beads aligned with the loading direction [47]. At least five areas were selected in each section for quantitative image analysis.

To produce sections transverse to the loading direction, the strips were carefully positioned on top of a layer of semi-polymerized resin. More resin was added to fully encapsulate the strips, and the assembly was sectioned perpendicular to the loading direction. During sectioning, the sample was positioned, so that the cutting direction aligned with the sample width. For sample thickness measurement, 0.5 µm sections of all samples were collected and then dried onto microscope coverslips. It should be noted that the fixation, dehydration and embedding process can cause sample shrinkage [48,49]. In this study, we did not adjust the thickness measurements for this shrinkage, because the extent of shrinkage for this particular material has not been measured.

2.6. Transmission electron microscope image post-processing

2.6.1. Area fraction

The greyscale TEM image of the transverse section was filtered using the adaptive Wiener two-dimensional noise removal filter and then converted into a binary image using Otsu's thresholding method (figure 3). Area fraction of the binary image was computed by normalizing the pixels occupied by the fibrils by the image size. For each specimen, we identified three image areas (4.4 × 4.4 µm^2) that were free of beads and edges for image analysis.

2.6.2. Fibril diameter distribution

The binary images of the transverse section were used to determine the fibril diameter distribution. For each fibril, the area as

Table 2. DDCS length and width with the corresponding normalized experimental parameters.

normalized experimental parameters				
displacement magnitude (mm)	1		2	
strain magnitude (%)	13.0 ± 1.1		26.7 ± 2.2	
strain rate during loading/unloading cycle	0.7 ± 0.1% per min		1.3 ± 0.1% per min	
strain rate during ramp to failure	0.7 ± 0.1% per min		0.7 ± 0.1% per min	
no. cycles	one (control)	50	one (control)	50
no. samples	6	6	6	6
DDCS length				
initial length (mm)	7.53 ± 0.66	7.78 ± 0.65	7.46 ± 0.60	7.62 ± 0.64
stress-free length after cyclic loading (mm)	7.80 ± 0.65	8.51 ± 0.66	8.29 ± 0.63	9.19 ± 0.64
% increase in length after cyclic loading	3.6 ± 0.6	9.4 ± 0.8	11. 2 ± 1.1	20.6 ± 1.8
DDCS width				
initial width (mm)	4.83 ± 0.23	4.99 ± 0.19	4.94 ± 0.58	4.93 ± 0.31
width after cyclic loading (mm)	4.81 ± 0.24	4.60 ± 0.20	4.76 ± 0.57	4.05 ± 0.38
% decrease in width after cyclic loading	0.5 ± 0.3	7.7 ± 3.2	3.8 ± 1.7	18.0 ± 3.9

well as minor axis and major axis diameters were determined (MATLAB function *regionprops*). The minor axis of each fibril was used to represent the actual fibril diameter [50,51]. Fibrils oriented within the plane of the section were excluded from the analysis. Other sources of error such as noise (minor diameter less than 25 nm) and large objects owing to unresolvable fibril boundaries (minor diameter larger than 500 nm, and compactness lower than 0.8) were also eliminated from the analysis. At least 500 fibril diameters were measured for each specimen.

2.6.3. Fibril orientation distribution

The Fourier transform method detailed in Sander & Barocas [52] was used to estimate the collagen fibril orientation distribution from the *en face* TEM images of the substrate. Briefly, the greyscale image was transformed into the frequency domain using a two-dimensional discrete Fourier transform. After applying a bandpass filter to remove high and low frequencies corresponding to potential image noise and uneven illumination, respectively, the frequency domain was transformed into polar coordinates to give the orientation distribution as a function of orientation angle. For each specimen prepared for TEM, the fibril orientation distributions were obtained from at least five images (each image corresponding to a DDCS area measuring $4.4 \times 4.4\ \mu m^2$). These distributions were pooled together to provide an estimate of the probability density function for the entire specimen. The mean, standard deviation and variance of the orientation angle was then estimated using circular statistics for bimodal distributions [52,53]. The mean angle of the distribution was defined as, $\mu = 1/2\ \tan^{-1}(b/a)$, where, $a = \sum_{i=1}^{i=N} f(\theta_i)\cos 2\theta_i / f(\theta_i)$, and $b = \sum_{i=1}^{i=N} f(\theta_i)\sin 2\theta_i / f(\theta_i)$. Here, $f(\theta_i)$ is the normalized frequency of the distribution. The standard deviation was defined using the equation, $s = [-\ln(R^{0.5})]^{0.5}$, where $R = \left(\sqrt{a^2 + b^2}\right)^{1/4}$ is the dispersion [53]. The dispersion is related to circular variance, $V = 1 - R$. In circular statistics, V ranges from 0 to 1. When V is close to 0, the distribution is purely isotropic, and when V is close to 1, the distribution is highly anisotropic.

2.6.4. Fibril periodicity

For each specimen, five fibrils with at least 500 nm of straight section where the banding period was visible were chosen in TEM images of the *en face* section. The greyscale pixel values on the fibril length were averaged over 20 rows. The one-dimensional averaged spatial signal was converted into the frequency domain using discrete Fourier transform, and the power spectral density plot was obtained. The fibril banding periodicity was identified by choosing the highest peak between the 60 and 80 nm period in the power spectral density. All image processing was performed in MATLAB.

2.7. Statistical analysis

Tukey–Kramer *post hoc* analysis of variance with a significance level of 5% was used to determine statistical significance. All statistical analyses were performed in MATLAB.

3. Results

3.1. Tissue geometry

An increase in the stress-free length was observed after cyclic loading in all samples. The extent of lengthening was significantly higher in the 50-cycle groups compared with the corresponding one-cycle controls ($p < 0.001$; table 2). The decrease in width after 50 cycles was significantly different from the one-cycle control for both displacement magnitudes ($p < 0.001$), but no difference was observed in the one-cycle control groups between the two cyclic strain levels. Sample thickness for all groups increased significantly compared with the initial sample thickness from 49.53 ± 11.65 ($n = 3$) to 88.64 ± 12.95 μm ($n = 12$), but it was not significantly different between groups. There was no statistically significant difference in sample thickness after cyclic loading between the 50-cycle and control groups (table 3). However, the thickness of all groups was significantly higher compared with the initial sample thickness (49.53 ± 11.65 μm, $n = 3$). This swelling was not caused by the application of loading, because the thickness of unloaded DDCS specimens stored under the same environmental conditions as the experimental groups for the duration of the cyclic loading (84.94 ±

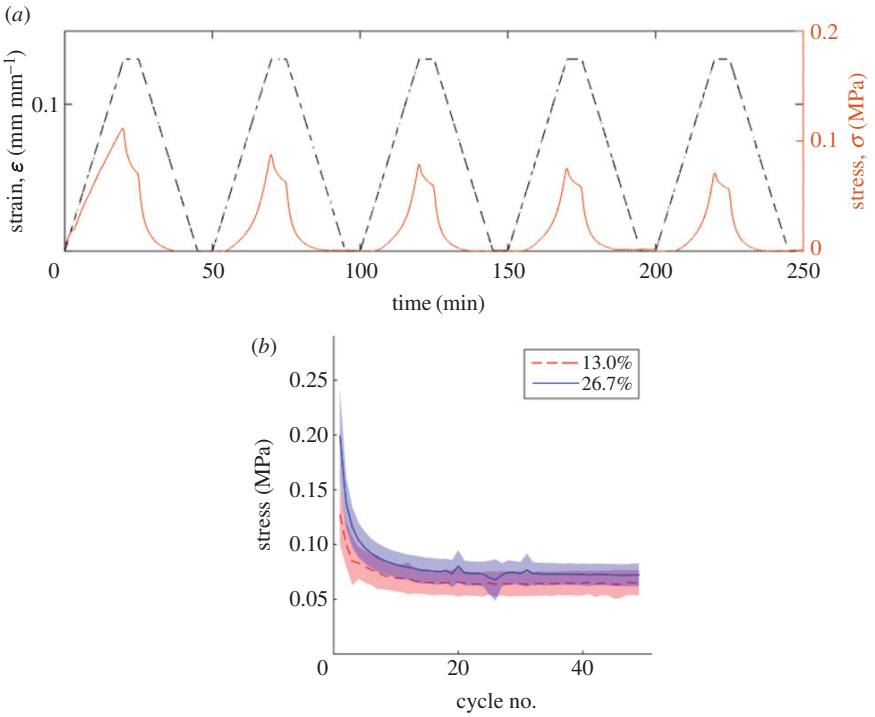

Figure 4. (*a*,*b*) The peak stress in each cycle is the value of maximum stress achieved in the loading step of a cycle, which decreased substantially within the first few cycles, and plateaued to a constant stress value for both strain levels (solid lines indicate average values and the corresponding shading indicates the standard deviation). (Online version in colour.)

Table 3. Collagen fibril periodic banding (average ± s.d.). No statistically significant difference was observed.

strain magnitude	13.0% (nm)	26.7% (nm)
after one cycle (control)	65.7 ± 2.4	67.2 ± 1.4
after 50 cycles	68.8 ± 4.3	66.6 ± 1.0

7.06 µm, $n = 3$) was not statistically different compared with the cyclic loading groups.

3.2. Cyclic loading response

During cyclic loading, the stress–strain curve shifted to the right with each cycle, as expected. The most substantial decrease in the stress amplitude of the cyclic response (37.13% and 51.2%, for the low and high strain levels, respectively) occurred during the first five cycles (figure 4). The stress amplitude decreased to a similar steady-state value, 0.065 ± 0.012 and 0.072 ± 0.011 MPa, for the two different applied strain amplitudes (figure 4). The degree of stress relaxation during the hold at the maximum displacement also decreased with each cycle and the stress-free length of the sample increased gradually during cyclic loading, and the largest increase in length occurred during the first few cycles (figure 5). These observations were consistent with preconditioning effects observed for uniaxial tension loading in the literature [13,14,54].

3.3. Mechanical properties of the dense, disorganized collagen substrate after cyclic loading

The mechanical response of DDCS was significantly altered by cyclic loading but less so by the amplitude of the imposed

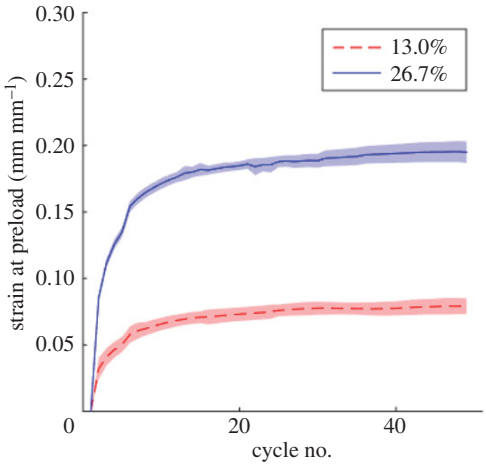

Figure 5. The strain at preload substantially increased within the first few cycles (solid lines indicate average values and the corresponding shading indicates the standard deviation). (Online version in colour.)

deformation (figure 6). Significant plastic lengthening in the 50-cycle groups drove the stress–stretch curve shift to the right. Remarkably, the 50-cycle groups demonstrated significantly higher ultimate stresses and steeper slopes compared with the single cycle control groups (figures 6 and 7). However, the ultimate stress was reached at a lower stretch value (figure 6).

3.4. Tissue microstructure after cyclic loading

Circular variance, which provides a measure of fibril alignment, was not significantly different between the 50-cycle and the one-cycle groups for 13.02% strain magnitude (figure 8). In contrast, 26.68% strain magnitude resulted in a

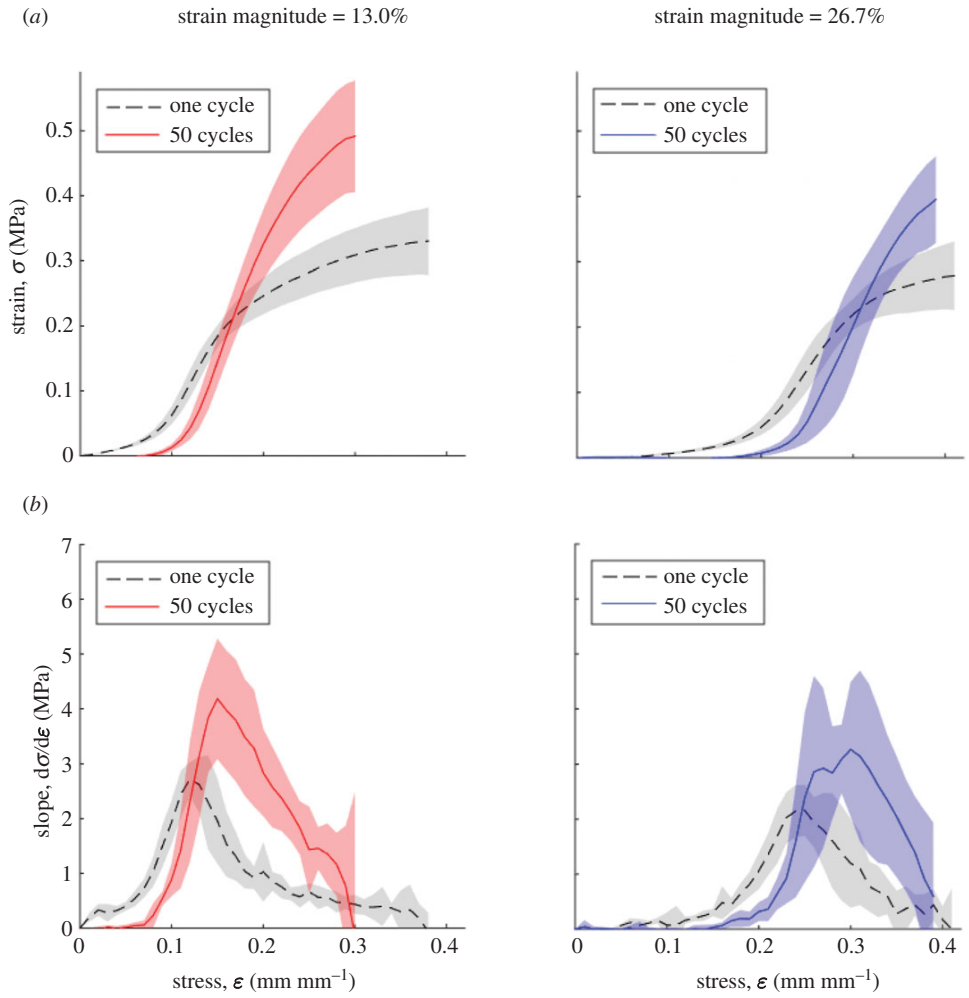

Figure 6. (*a*) DDCS stress–strain curve (average ± s.d.) after cyclic loading and the corresponding (*b*) derivative of the curve. Stress and strain were normalized against initial DDCS geometry before cyclic loading. (Online version in colour.)

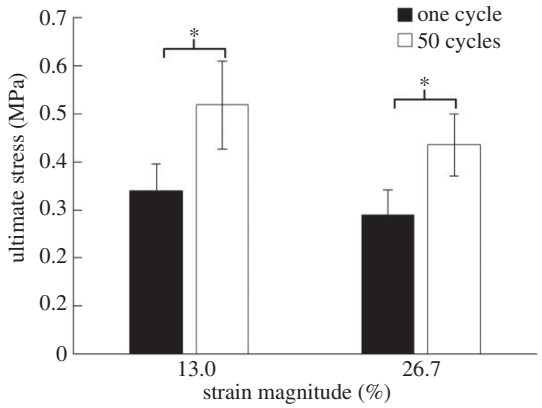

Figure 7. Ultimate tensile strength of the DDCS after cyclic loading. *$p < 0.01$.

significantly lower variance in the distribution after 50 cycles (figure 8). A mean angle of 15.8 ± 11.1° from the loading direction was calculated for the 50-cycle group, which indicates that collagen fibrils reoriented towards the direction of loading. Despite the significant differences in sample geometry after the application of cyclic loading in different groups, there was no statistically significant difference in the area fraction of the cross section (figure 9), or in the periodic banding between groups (table 3). There was no significant difference in the mean fibril diameter between the single cycle and 50-cycle groups (table 4).

4. Discussion

Previous studies have shown that the mechanical properties of connective soft tissues are time and loading history-dependent. However, the mechanism that generates this behaviour is still not well understood. This study measured the effect of cyclic loading at two different strain amplitudes on the mechanical properties, as well as the microstructure, of a dense collagenous substrate. In agreement with the preconditioning effects widely observed in biological tissues and engineered collagen constructs [13–16], the DDCS also showed the shift of the stress–strain curve and decrease in peak force during cyclic loading. In addition, the DDCS also showed the preconditioning-induced strengthening through a significant increase in ultimate strength, similar to that observed in tendons [17,18,21], ligaments [17,18] and collagen gel [22]. The increase in ultimate strength occurred at both strain levels. As discussed in the Methods section, while the lower strain level was selected because it

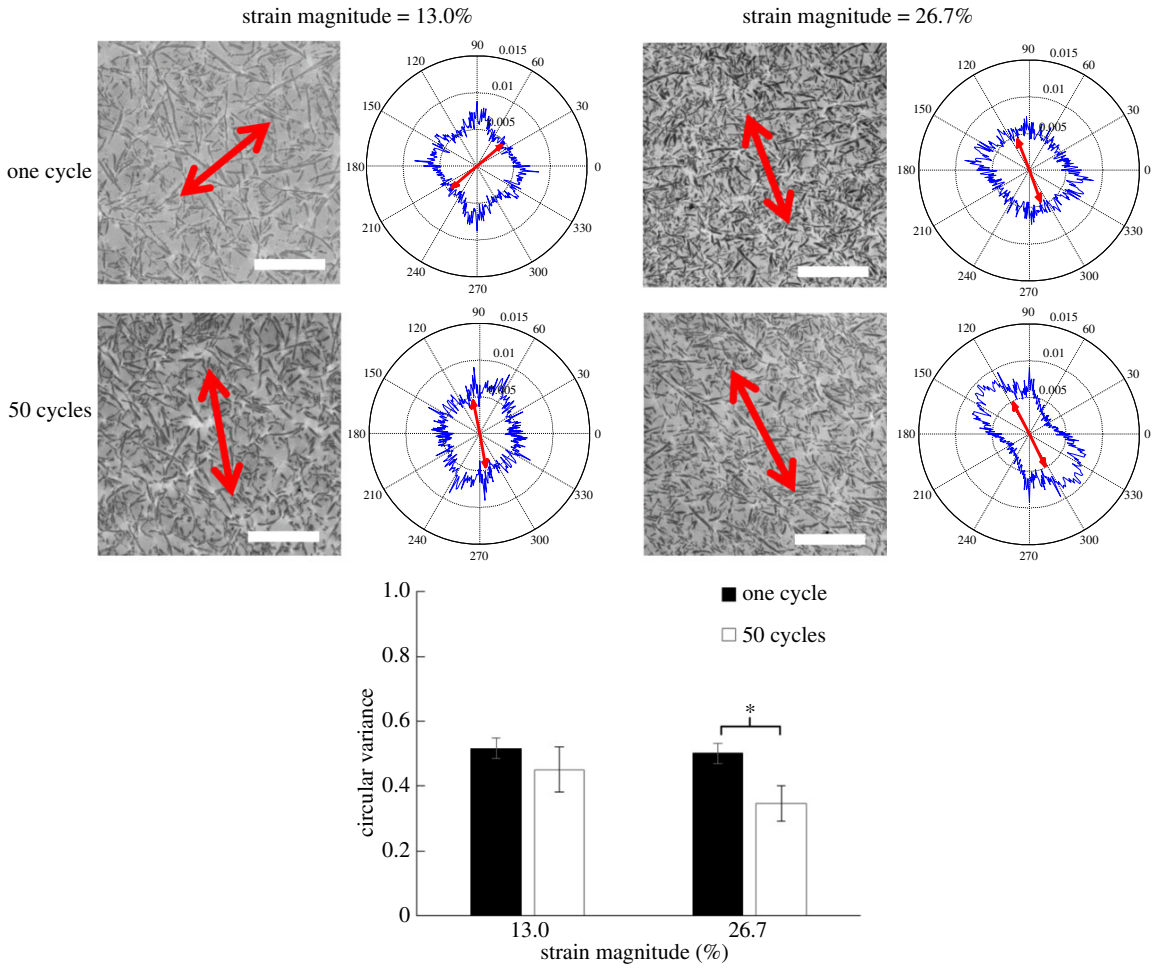

Figure 8. Representative TEM images of the *en face* section (red arrow represents the loading direction and scale bar, 5 µm) with the fibril orientation distribution polar plots and summary of circular variance of the orientation distribution after cyclic loading. $*p < 0.02$. (Online version in colour.)

resides within the linear region and well below failure, the higher strain level was chosen because it represents the point where damage is likely to start occurring. Our results are inconsistent with the finding in [23], where the ultimate strength of tendon tissue decreased as a result of preconditioning with a strain magnitude close to the failure strain. This difference might be due to the uncross-linked nature of the DDCS, where molecular mobility is less constrained compared with the cross-linked collagen in native tendon.

Cyclic loading also altered the specimens' geometry: the stress-free length was increased and the width was decreased. Increase in stress-free length from cyclic loading has been observed in other studies involving native soft tissue, but the extent of lengthening can be exacerbated by the removal of proteoglycan [14] or the addition of an isometric hold during cyclic loading [55]. Despite this substantial change in sample geometry, cyclic loading did not significantly change the cross-sectional area fraction and fibril orientation only changed significantly in the higher strain level group. These observations suggest that the increase in the tangent modulus and strength in both cycled samples was not attributed to fibril crowding or realignment with the loading direction. The lack of reorientation observed at the lower strain level is likely, because each cycle in our experiment allowed the specimen to return to zero displacement. Tendon and tissue equivalents have been shown to recover their fibril orientation distribution after preconditioning and stress relaxation if the tissue was unloaded to zero displacement, instead of preload [24,25] with a recovery time as short as 60 s [25].

In contrast to Cheema *et al.*, we found no effect of cyclic loading on the fibril diameter distribution. Cheema *et al.* [22] reports fibril diameter increases, possibly due to fusion of multiple smaller fibrils. The DDCS used in our investigation has undergone tremendous compression during fabrication when it was dehydrated by dialysing against 40% polyethylene glycol for 24 h, possibly pre-fusing the fibrils.

Other than the fibril spatial distribution and diameter, two other factors that determine the mechanical properties of entangled fibrillar network include the degree of interfibrillar bonding or friction and the mechanical properties of the fibrils [40]. The interfibrillar contact rupture and reconnection was proposed as a possible mechanism for the increase in ultimate shear stress following cyclic shear loading observed in the actin network with cross-linking proteins [56]. Even though this study did not include a cross-linking agent in the medium during cyclic loading, it is unclear whether the strength or quantity of interfibrillar connections in the DDCS was altered by cyclic loading. The change in fibril mechanical

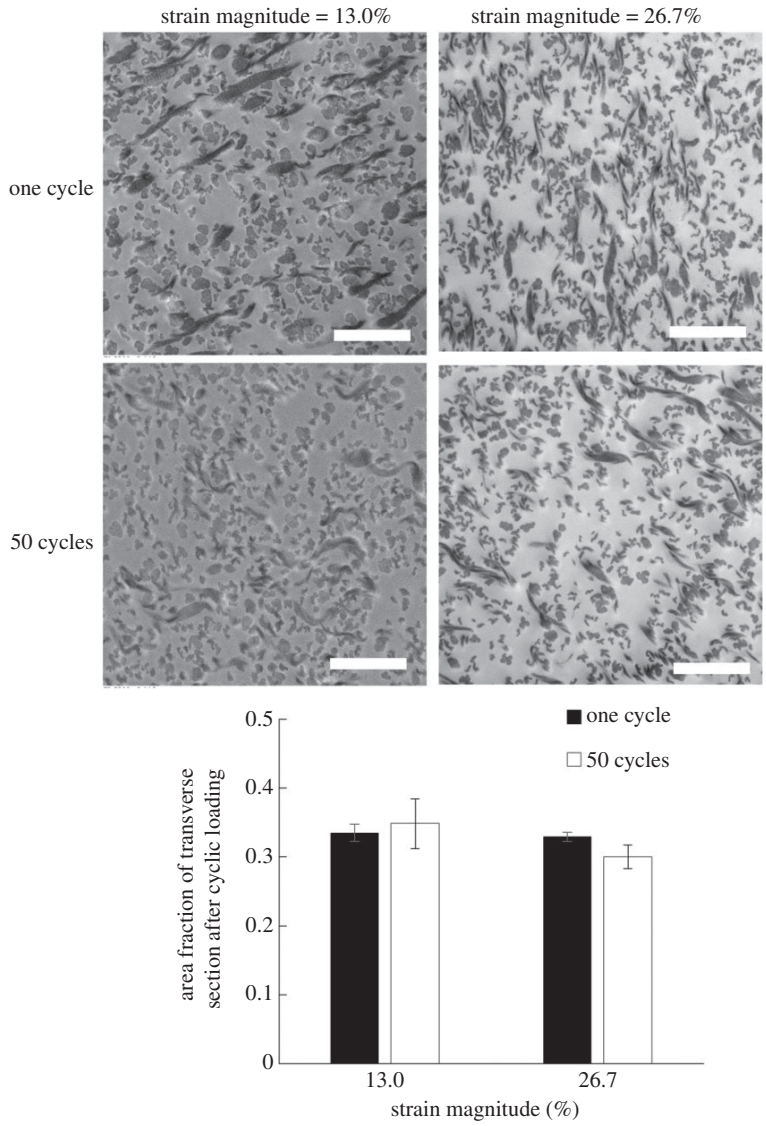

Figure 9. Representative TEM images of the transverse section (scale bar, 1 μm) and summary of area fraction of the DDCS cross section after cyclic loading. No statistically significant difference was observed.

Table 4. Mean fibril diameter (average ± s.d., $n = 3$ for each group). No statistically significant difference was observed.

strain magnitude	13.0% (nm)	26.7% (nm)
after one cycle (control)	78.1 ± 3.4	77.0 ± 7.4
after 50 cycles	82.9 ± 3.3	75.6 ± 4.5

properties into a more brittle-like material with a higher fracture stress was demonstrated in a molecular model proposed by Buehler [57] by an increase in adhesion between collagen molecules. Future investigation of the effect of cyclic loading on interfibrillar and intrafibrillar bonding can provide a more definite theory regarding the mechanism involved in changing the mechanical properties of soft connective tissues.

Biological tissues are viscoelastic materials. The rate of strain in soft tissues has been found to increase the tangent modulus when the strain rate was increased [54,58–66], which can generate a more severe stress relaxation response as a higher peak stress is reached at the beginning of the stress relaxation period [55]. The low displacement rates for this investigation were deliberately selected to reduce the viscoelastic effects of the DDCS. In addition, because our principal findings compare material properties measured on different samples using the same method, we do not expect small viscoelastic effects to influence the results appreciably. Failure to permit an adequate viscoelastic recovery time between testing events can lead to apparent increases in the zero-load strain and apparent increases in the tangent modulus. Previous investigations in the literature have used a range of recovery times, from the order of hundreds of seconds [14,67] to hours [23] to days [68]. In this investigation, a 5-min hold at zero displacement was prescribed between events. However, because the specimens unloaded to a stress-free state (force is lower than preload) well before they reached zero displacement, the recovery time was extended. In the next cycle, the specimen also did not reach the preload immediately. As a result, the effective period where the specimen was stress-free was much longer than the 5-min period of zero displacement. Between the 49th and 50th cycle, the stress-free period can be as long as

34 ± 3 and 38 ± 1 min, for the lower and higher strain levels, respectively. As a comparison, the time constant of the 50th cycle's stress relaxation was 1.8 ± 0.3 min, when the data were curve fitted to the Maxwell–Weichert model [69,70]. Because the recovery time was approximately 20 times the stress relaxation time constant, the material had adequate time to recover prior to the next event. Given our experimental approach, we do not expect viscoelastic material behaviour to significantly affect our results.

This study presents the mechanical and microstructural analysis of dense collagenous substrates after cyclic loading. TEM imaging provides direct visualization of the substrate's microstructure. Results of this study suggest that the mechanical strengthening from cyclic loading of uncross-linked collagenous substrates did not arise only from collagen fibril alignment towards the direction of load. This suggests that mechanical loading induces stabilizing changes internal to the fibrils themselves or in the fibril–fibril interactions. Resolving the source of this phenomenon is an important step towards understanding how biological tissues are maintained *in vivo*.

Data accessibility. Data available from the Dryad Digital Repository: doi:10.5061/dryad.tr2f1.

Competing interests. We declare we have no competing interests.

Funding. T.D.N. acknowledges funding from NSF Career Award CMMI: 1253453. E.A.S. acknowledges funding from NSF Career Award CMMI: 1452728.

Acknowledgements. Research reported in this publication was supported by the National Eye Institute of the National Institutes of Health under NIH/NEI (R01) EY0015500.

References

1. Kongsgaard M, Aagaard P, Kjaer M, Magnusson SP. 2005 Structural Achilles tendon properties in athletes subjected to different exercise modes and in Achilles tendon rupture patients. *J. Appl. Physiol.* **99**, 1965–1971. (doi:10.1152/japplphysiol.00384.2005)
2. Kongsgaard M, Reitelseder S, Pedersen TG, Holm L, Aagaard P, Kjaer M, Magnusson SP. 2007 Region specific patellar tendon hypertrophy in humans following resistance training. *Acta Physiol.* **191**, 111–121. (doi:10.1111/j.1748-1716.2007.01714.x)
3. Woo SL, Ritter MA, Amiel D, Sanders TM, Gomez MA, Kuei SC, Garfin SR, Akeson WH. 1980 The biomechanical and biochemical properties of swine tendons: long term effects of exercise on the digital extensors. *Connect. Tissue Res.* **7**, 177–183. (doi:10.3109/03008208009152109)
4. Fung DT *et al.* 2010 Early response to tendon fatigue damage accumulation in a novel *in vivo* model. *J. Biomech.* **43**, 274–279. (doi:10.1016/j.jbiomech.2009.08.039)
5. Arya S, Kulig K. 2010 Tendinopathy alters mechanical and material properties of the Achilles tendon. *J. Appl. Physiol.* **108**, 670–675. (doi:10.1152/japplphysiol.00259.2009)
6. de Boer MD *et al.* 2007 The temporal responses of protein synthesis, gene expression and cell signalling in human quadriceps muscle and patellar tendon to disuse. *J. Physiol.* **585**, 241–251. (doi:10.1113/jphysiol.2007.142828)
7. Neath P, Roche SM, Bee JA. 1991 Intraocular pressure-dependent and -independent phases of growth of the embryonic chick eye and cornea. *Invest. Ophthalmol. Vis. Sci.* **32**, 2483–2491.
8. Bayer ML *et al.* 2010 The initiation of embryonic-like collagen fibrillogenesis by adult human tendon fibroblasts when cultured under tension. *Biomaterials* **31**, 4889–4897. (doi:10.1016/j.biomaterials.2010.02.062)
9. Miller BF *et al.* 2005 Coordinated collagen and muscle protein synthesis in human patella tendon and quadriceps muscle after exercise. *J. Physiol.* **567**, 1021–1033. (doi:10.1113/jphysiol.2005.093690)
10. Butt RP, Bishop JE. 1997 Mechanical load enhances the stimulatory effect of serum growth factors on cardiac fibroblast procollagen synthesis. *J. Mol. Cell. Cardiol.* **29**, 1141–1151. (doi:10.1006/jmcc.1996.0347)
11. Robbins JR, Evanko SP, Vogel KG. 1997 Mechanical loading and TGF-beta regulate proteoglycan synthesis in tendon. *Arch. Biochem. Biophys.* **342**, 203–211. (doi:10.1006/abbi.1997.0102)
12. Prajapati RT, Chavally-Mis B, Herbage D, Eastwood M, Brown RA. 2000 Mechanical loading regulates protease production by fibroblasts in three-dimensional collagen substrates. *Wound Repair Regen.* **8**, 226–237. (doi:10.1046/j.1524-475x.2000.00226.x)
13. Fung YC. 1981 *Biomechanics: mechanical properties of living tissues*, pxii, 433 pp. New York, NY: Springer.
14. Eshel H, Lanir Y. 2001 Effects of strain level and proteoglycan depletion on preconditioning and viscoelastic responses of rat dorsal skin. *Ann. Biomed. Eng.* **29**, 164–172. (doi:10.1114/1.1349697)
15. Sverdlik A, Lanir Y. 2002 Time-dependent mechanical behavior of sheep digital tendons, including the effects of preconditioning. *J. Biomech. Eng.* **124**, 78–84. (doi:10.1115/1.1427699)
16. Quinn KP, Winkelstein BA. 2011 Preconditioning is correlated with altered collagen fiber alignment in ligament. *J. Biomech. Eng.* **133**, 064506. (doi:10.1115/1.4004205)
17. Schatzmann L, Brunner P, Staubli HU. 1998 Effect of cyclic preconditioning on the tensile properties of human quadriceps tendons and patellar ligaments. *Knee Surg. Sports Traumatol. Arthrosc.* **6**(Suppl. 1), S56–S61. (doi:10.1007/s001670050224)
18. Su WR, Chen HH, Luo ZP. 2008 Effect of cyclic stretching on the tensile properties of patellar tendon and medial collateral ligament in rat. *Clin. Biomech. (Bristol, Avon)* **23**, 911–917. (doi:10.1016/j.clinbiomech.2008.04.002)
19. Sellaro TL, Hildebrand D, Lu Q, Vyavahare N, Scott M, Sacks MS. 2007 Effects of collagen fiber orientation on the response of biologically derived soft tissue biomaterials to cyclic loading. *J. Biomed. Mater. Res. A* **80**, 194–205. (doi:10.1002/jbm.a.30871)
20. Tonge TK, Murienne BJ, Coudrillier B, Alexander S, Rothkopf W, Nguyen TD. 2013 Minimal preconditioning effects observed for inflation tests of planar tissues. *J. Biomech. Eng.* **135**, 114502. (doi:10.1115/1.4025105)
21. Teramoto A, Luo ZP. 2008 Temporary tendon strengthening by preconditioning. *Clin. Biomech. (Bristol, Avon)* **23**, 619–622. (doi:10.1016/j.clinbiomech.2007.12.001)
22. Cheema U, Chuo CB, Sarathchandra P, Nazhat SN, Brown RA. 2007 Engineering functional collagen scaffolds: cyclical loading increases material strength and fibril aggregation. *Adv. Funct. Mater.* **17**, 2426–2431. (doi:10.1002/adfm.200700116)
23. Legerlotz K, Riley GP, Screen HR. 2013 GAG depletion increases the stress-relaxation response of tendon fascicles, but does not influence recovery. *Acta Biomater.* **9**, 6860–6866. (doi:10.1016/j.actbio.2013.02.028)
24. Tower TT, Neidert MR, Tranquillo RT. 2002 Fiber alignment imaging during mechanical testing of soft tissues. *Ann. Biomed. Eng.* **30**, 1221–1233. (doi:10.1114/1.1527047)
25. Miller KS, Edelstein L, Connizzo BK, Soslowsky LJ. 2012 Effect of preconditioning and stress relaxation on local collagen fiber re-alignment: inhomogeneous properties of rat supraspinatus tendon. *J. Biomech. Eng.* **134**, 031007. (doi:10.1115/1.4006340)
26. Waller JM, Maibach HI. 2006 Age and skin structure and function, a quantitative approach (II): protein, glycosaminoglycan, water, and lipid content and structure. *Skin Res. Technol.* **12**, 145–154. (doi:10.1111/j.0909-752X.2006.00146.x)
27. Neuman RE, Logan MA. 1950 The determination of collagen and elastin in tissues. *J. Biol. Chem.* **186**, 549–556.
28. Newsome DA, Gross J, Hassell JR. 1982 Human corneal stroma contains three distinct collagens. *Invest. Ophthalmol. Vis. Sci.* **22**, 376–381.

29. Keeley FW, Morin JD, Vesely S. 1984 Characterization of collagen from normal human sclera. *Exp. Eye Res.* **39**, 533–542. (doi:10.1016/0014-4835(84)90053-8)
30. Lotz JC, Hadi T, Bratton C, Reiser KM, Hsieh AH. 2008 Anulus fibrosus tension inhibits degenerative structural changes in lamellar collagen. *Eur. Spine J.* **17**, 1149–1159. (doi:10.1007/s00586-008-0721-y)
31. Flynn BP, Bhole AP, Saeidi N, Liles M, Dimarzio CA, Ruberti JW. 2010 Mechanical strain stabilizes reconstituted collagen fibrils against enzymatic degradation by mammalian collagenase matrix metalloproteinase 8 (MMP-8). *PLoS ONE* **5**, e12337. (doi:10.1371/journal.pone.0012337)
32. Bhole AP, Flynn BP, Liles M, Saeidi N, Dimarzio CA, Ruberti JW. 2009 Mechanical strain enhances survivability of collagen micronetworks in the presence of collagenase: implications for load-bearing matrix growth and stability. *Phil. Trans. R. Soc. A* **367**, 3339–3362. (doi:10.1098/rsta.2009.0093)
33. Zareian R, Church KP, Saeidi N, Flynn BP, Beale JW, Ruberti JW. 2010 Probing collagen/enzyme mechanochemistry in native tissue with dynamic, enzyme-induced creep. *Langmuir* **26**, 9917–9926. (doi:10.1021/la100384e)
34. Ruberti JW, Hallab NJ. 2005 Strain-controlled enzymatic cleavage of collagen in loaded matrix. *Biochem. Biophys. Res. Commun.* **336**, 483–489. (doi:10.1016/j.bbrc.2005.08.128)
35. Camp RJ, Liles M, Beale J, Saeidi N, Flynn BP, Moore E, Murthy SK, Ruberti JW. 2011 Molecular mechanochemistry: low force switch slows enzymatic cleavage of human type I collagen monomer. *J. Am. Chem. Soc.* **133**, 4073–4078. (doi:10.1021/ja110098b)
36. Nabeshima Y, Grood ES, Sakurai A, Herman JH. 1996 Uniaxial tension inhibits tendon collagen degradation by collagenase *in vitro*. *J. Orthop. Res.* **14**, 123–130. (doi:10.1002/jor.1100140120)
37. Wells PB, Thomsen S, Jones MA, Baek S, Humphrey JD. 2005 Histological evidence for the role of mechanical stress in modulating thermal denaturation of collagen. *Biomech. Model. Mechanobiol.* **4**, 201–210. (doi:10.1007/s10237-005-0002-1)
38. Lennox FG. 1947 Shrinkage of collagen. *Biochem. J.* **41**, pxivii.
39. Kabla A, Mahadevan L. 2007 Nonlinear mechanics of soft fibrous networks. *J. R. Soc. Interface* **4**, 99–106. (doi:10.1098/rsif.2006.0151)
40. Picu RC. 2011 Mechanics of random fiber networks: a review. *Soft Matter* **7**, 6768–6785. (doi:10.1039/c1sm05022b)
41. Pritchard RH, Huang YY, Terentjev EM. 2014 Mechanics of biological networks: from the cell cytoskeleton to connective tissue. *Soft Matter* **10**, 1864–1884. (doi:10.1039/c3sm52769g)
42. Elliott DM, Narmoneva DA, Setton LA. 2002 Direct measurement of the Poisson's ratio of human patella cartilage in tension. *J. Biomech. Eng.* **124**, 223–228. (doi:10.1115/1.1449905)
43. Roeder BA, Kokini K, Sturgis JE, Robinson JP, Voytik-Harbin SL. 2002 Tensile mechanical properties of three-dimensional type I collagen extracellular matrices with varied microstructure. *J. Biomech. Eng.* **124**, 214–222. (doi:10.1115/1.1449904)
44. Silver FH, Christiansen DL, Snowhill PB, Chen Y. 2000 Role of storage on changes in the mechanical properties of tendon and self-assembled collagen fibers. *Connect. Tissue Res.* **41**, 155–164. (doi:10.3109/03008200009067667)
45. Paten JA, Zareian R, Saeidi N, Melotti SA, Ruberti JW. 2011 Design and performance of an optically accessible, low-volume, mechanobioreactor for long-term study of living constructs. *Tissue Eng. Part C, Methods* **17**, 775–788. (doi:10.1089/ten.TEC.2010.0642)
46. Meghezi S, Couet F, Chevallier P, Mantovani D. 2012 Effects of a pseudophysiological environment on the elastic and viscoelastic properties of collagen gels. *Int. J. Biomater.* **2012**, 319290. (doi:10.1155/2012/319290)
47. Jesior JC. 1985 How to avoid compression: a model study of latex sphere grid sections. *J. Ultrastruct. Res.* **90**, 135–144. (doi:10.1016/0889-1605(85)90104-1)
48. Fullwood NJ, Meek KM. 1993 A synchroton X-ray study of the changes occurring in the corneal stroma during processing for electron microscopy. *J. Microsc.* **169**, 53–60. (doi:10.1111/j.1365-2818.1993.tb03277.x)
49. Hanstede JG, Gerrits PO. 1983 The effects of embedding in water-soluble plastics on the final dimensions of liver sections. *J. Microsc.* **131**, 79–86. (doi:10.1111/j.1365-2818.1983.tb04233.x)
50. Lavagnino M, Arnoczky SP, Frank K, Tian T. 2005 Collagen fibril diameter distribution does not reflect changes in the mechanical properties of *in vitro* stress-deprived tendons. *J. Biomech.* **38**, 69–75. (doi:10.1016/j.jbiomech.2004.03.035)
51. Christiansen DL, Huang EK, Silver FH. 2000 Assembly of type I collagen: fusion of fibril subunits and the influence of fibril diameter on mechanical properties. *Matrix Biol.* **19**, 409–420. (doi:10.1016/S0945-053X(00)00089-5)
52. Sander EA, Barocas VH. 2009 Comparison of 2D fiber network orientation measurement methods. *J. Biomed. Mater. Res. A* **88**, 322–331. (doi:10.1002/jbm.a.31847)
53. Mardia KV, Jupp PE. 2000 *Directional statistics*, pxxi, 429 p. Chichester, UK: J. Wiley.
54. Boyce BL, Jones RE, Nguyen TD, Grazier JM. 2007 Stress-controlled viscoelastic tensile response of bovine cornea. *J. Biomech.* **40**, 2367–2376. (doi:10.1016/j.jbiomech.2006.12.001)
55. Fukaya H, Martin CJ, Young AC, Katsura S. 1968 Mechanical properties of alveolar walls. *J. Appl. Physiol.* **25**, 689–695.
56. Schmoller KM, Fernandez P, Arevalo RC, Blair DL, Bausch AR. 2010 Cyclic hardening in bundled actin networks. *Nat. Commun.* **1**, 134. (doi:10.1038/ncomms1134)
57. Buehler MJ. 2008 Nanomechanics of collagen fibrils under varying cross-link densities: atomistic and continuum studies. *J. Mech. Behav. Biomed. Mater.* **1**, 59–67. (doi:10.1016/j.jmbbm.2007.04.001)
58. Elsheikh A, Kassem W, Jones SW. 2011 Strain-rate sensitivity of porcine and ovine corneas. *Acta Bioeng. Biomech. Wroclaw Univ. Technol.* **13**, 25–36.
59. Zhou B, Xu F, Chen CQ, Lu TJ. 2010 Strain rate sensitivity of skin tissue under thermomechanical loading. *Phil. Trans. R. Soc. A* **368**, 679–690. (doi:10.1098/rsta.2009.0238)
60. Lim J, Hong J, Chen WNW, Weerasooriya T. 2011 Mechanical response of pig skin under dynamic tensile loading. *Int. J. Impact Eng.* **38**, 130–135. (doi:10.1016/j.ijimpeng.2010.09.003)
61. Silver FH, Ebrahimi A, Snowhill PB. 2002 Viscoelastic properties of self-assembled type I collagen fibers: molecular basis of elastic and viscous behaviors. *Connect. Tissue Res.* **43**, 569–580. (doi:10.1080/03008200290001302)
62. Haut TL, Haut RC. 1997 The state of tissue hydration determines the strain-rate-sensitive stiffness of human patellar tendon. *J. Biomech.* **30**, 79–81. (doi:10.1016/S0021-9290(96)00108-X)
63. Snedeker JG, Niederer P, Schmidlin FR, Farshad M, Demetropoulos CK, Lee JB, Yang KH. 2005 Strain-rate dependent material properties of the porcine and human kidney capsule. *J. Biomech.* **38**, 1011–1021. (doi:10.1016/j.jbiomech.2004.05.036)
64. Lynch HA, Johannessen W, Wu JP, Jawa A, Elliott DM. 2003 Effect of fiber orientation and strain rate on the nonlinear uniaxial tensile material properties of tendon. *J. Biomech. Eng.* **125**, 726–731. (doi:10.1115/1.1614819)
65. Nguyen TD, Jones RE, Boyce BL. 2008 A nonlinear anisotropic viscoelastic model for the tensile behavior of the corneal stroma. *J. Biomech. Eng.* **130**, 041020. (doi:10.1115/1.2947399)
66. Nguyen TD, Jones RE, Boyce BL. 2007 Modeling the anisotropic finite-deformation viscoelastic behavior of soft fiber-reinforced composites. *Int. J. Solids Struct.* **44**, 8366–8389. (doi:10.1016/j.ijsolstr.2007.06.020)
67. Duenwald SE, Vanderby Jr R, Lakes RS. 2010 Stress relaxation and recovery in tendon and ligament: experiment and modeling. *Biorheology* **47**, 1–14. (doi:10.3233/BIR-2010-0559)
68. Carew EO, Garg A, Barber JE, Vesely I. 2004 Stress relaxation preconditioning of porcine aortic valves. *Ann. Biomed. Eng.* **32**, 563–572. (doi:10.1023/B:ABME.0000019176.49650.19)
69. Paten JA, Tilburey GE, Molloy EA, Zareian R, Trainor CV, Ruberti JW. 2013 Utility of an optically-based, micromechanical system for printing collagen fibers. *Biomaterials* **34**, 2577–2587. (doi:10.1016/j.biomaterials.2012.12.028)
70. Shen ZL, Kahn H, Ballarini R, Eppell SJ. 2011 Viscoelastic properties of isolated collagen fibrils. *Biophys. J.* **100**, 3008–3015. (doi:10.1016/j.bpj.2011.04.052)